

Air Free-Cooled Tropical Data Center: Design, Evaluation, and Learned Lessons

Duc Van Le, Yingbo Liu, Rongrong Wang, Rui Tan, and Lek Heng Ngoh

Abstract—Air free cooling is an energy-efficient cooling scheme that has been adopted in the dry and cold climate zones. To adopt this cooling scheme in Singapore’s tropical condition, we designed and implemented an air free-cooled DC testbed integrating sensing and control systems for the server and room conditions. Then, we conducted extensive experiments on the testbed to understand its energy efficiency and server reliability. This paper presents the key observations, experiences, and learned lessons obtained from our testbed over a duration of nearly two years. The experiments show that (1) the air free-cooling design can achieve the power usage effectiveness of 1.05, (2) the tropics’ year-round high temperatures up to 37°C do not impede the air free-cooling, and (3) the implementation of the air free-cooled tropical DCs requires special cares to deal with airborne contaminants to avoid fast corrosion rate and dust-induced server faults. Based on our experiment data, a set of recommendations on the temperature control and the selection of IT equipment for air free-cooled tropical DCs is made. The descriptions of the learned lessons, the resulting recommendations, and the released data can be useful to the relevant research communities, governmental agencies, and standardizing bodies.

Index Terms—Data center, green computing, free cooling, performance, reliability, energy sustainability

1 INTRODUCTION

Singapore is a growing digital hub which hosts about 60% of the Southeast Asia’s data center (DC) market [2] and is projected to grow rapidly [3]. The impact of Singapore’s DC industry on the country’s energy sustainability has been a matter closely studied and monitored. In particular, Singapore’s tropical climate with year-round high temperatures and relative humidity (RH) levels introduces challenges for the local DC operators in improving the energy efficiency of their infrastructures. As a result, Singapore’s DCs spend more energy in cooling, compared with many other locations in the world. Thus, technologies and solutions that can improve DC energy efficiency in the tropics will further enhance Singapore’s attractiveness as a regional DC hub. They are also important to Singapore’s overall energy sustainability.

Air free-cooling that utilizes outside cold air to cool the information technology (IT) equipment has been increasingly used to improve the energy efficiency of DCs [4]. However, air free cooling in the tropics has been long thought infeasible from the intuition that the high temperature and relative humidity (RH) of the air supplied to the servers will undermine their performance and reliability. On the other hand, the American Society of Heating, Refrigeration and Air-Conditioning Engineers (ASHRAE) has been working

for years on expanding the suggested allowable temperature and RH ranges for IT equipment. For instance, the servers compliant with ASHRAE’s Class A3 [5] can operate continuously and reliably when the temperature and RH of the supply air are up to 40°C and 85%, respectively. This sheds light on the possibility of air free-cooled DCs in tropical climate since the maximum record temperature in our tropical region, i.e., Singapore, is 37°C and the ambient RH is in general lower than 90%.

However, the ASHRAE’s relaxed temperature and RH requirements are for traditional DCs that recirculate the clean air within the enclosed DC building. The air free-cooled DCs that continuously bring the outside air into the server rooms will introduce extra challenges due to various affecting factors such as the ambient temperature and RH, air volume flow rate, and cleanness level of the supply air. Therefore, it is essential to investigate the details of how the affecting factors of tropical environment conditions will affect DC power usage, and the computing performance and reliability of the IT equipment. To achieve the goal, together with multiple partners in DC industry and research, we designed, constructed, and experimented with an air free-cooled DC testbed consisting of three server rooms located in two DC operators’ premises that are located in Singapore. The testbed hosts 12 server racks with 60 kW total power rating. We have conducted 18-month experiments on the built testbed, in which the cooling conditions (e.g., cold aisle temperature and air flow rate setpoints) and the server operating parameters (e.g., CPU utilization, hard disk drive (HDD) read/write speed, and memory copying parameters) are controlled in specified ranges. During the experiments, various types of sensor data, including environmental, energy, performance, and reliability measurements are collected to analyze the impact of different environmental conditions on DC energy efficiency, hardware reliability, and computing performance.

Duc Van Le, Rongrong Wang, and Rui Tan are with Nanyang Technological University, 50 Nanyang Avenue, Singapore, 639798, emails: {vdle,rrwang,tanrui}@ntu.edu.sg

Yingbo Liu is with Yunnan University of Finance and Economics, Yunnan, Kunming 650221, China. This work was completed when he was a Research Fellow at Nanyang Technological University, Singapore, email: liuyb@ynufe.edu.cn

Lek Heng Ngoh is with Info-communications Media Development Authority, Singapore, email: ngoh_lek_heng@imda.gov.sg

A preliminary version [1] of this work appeared in The 7th ACM International Conference on Systems for Energy-Efficient Buildings, Cities, and Transportation (BuildSys) held in Virtual Event, Japan, November 2020.

Several major DC operators including Facebook [6] and Google [7] have used the air free-cooling to improve the energy efficiency of their DCs, especially in cold and dry locations. However, they do not release the technical details. Several works [8]–[14] have studied the effectiveness of the air free-cooling in various climates throughout the world. However, those studies are mainly based on the analysis/simulations or small-scale testbeds. In this work, we study a basic problem of determining the environmental condition boundary at which the air free-cooled DC can operate without significant degradation of server performance and reliability while maximizing the use of air free-cooling to reduce the cooling energy usage in the tropics. To achieve the goal, we conduct a set of experiments on the real air free-cooled DC testbed to investigate the details of how the realistic tropical environment conditions affect DC power usage, computing throughput, and server hardware reliability. Specifically, from our experiments, we draw the key observations, experiences, learned lessons, and recommendations as follows.

- 1) The air free-cooling design that uses fans to control the volume flow rate of the outside air supplied to the servers can reduce the power usage effectiveness (PUE)¹ by 38%, compared with the global average PUE of 1.7 [15].
- 2) The servers can operate without computing performance degradation under combined impact of various realistic factors, including temperature up to 37°C and RH above 90%. In other words, the tropics' year-round high temperatures up to 37°C do not impede the air free-cooling in the tropics.
- 3) The implementation of the air free-cooled DCs in tropics requires special cares to deal with airborne contaminants to avoid fast corrosion rate and dust-induced server faults.
- 4) The existing DCs operated in enclosed buildings can increase their temperature setpoints for better energy efficiency without degrading server computing performance.
- 5) A set of recommendations on the temperature control and the selection of IT equipment for the air free-cooled DCs in the tropical climate zones is made based on the analysis using our collected data.
- 6) A set of collected data traces on energy usage and environment conditions is made publicly available. To the best of our knowledge, our released dataset² is the first of this kind, whereas other public DC-related datasets (e.g., Google's [16] and Alibaba's [17]) are merely about server workloads. More details can be found in Appendix A³.

The remainder of this paper is organized as follows. Section 2 presents background about the air free cooling and related works. Section 3 describes the design and construction of the testbed. Section 4 presents the experiments on

the testbed and the key results of server performance and energy usage. Section 5 details the IT equipment failures occurred during the course of the experiments. Section 6 presents the learned lessons and recommendations. Section 7 concludes this paper.

2 BACKGROUND AND RELATED WORK

2.1 Free-Cooling Systems for DCs

Free-cooling has been introduced as an effective technique to save the DC's cooling energy usage [4]. It directly uses the outside air to cool the servers and therefore reduce the need of power-hungry traditional cooling devices such as chillers and compressors [18]. Free-cooling has been implemented in two major forms which are air-side and water-side economizers [19]. The water-side economizer first uses the *computer room air conditioning* (CRAC) unit to circulate the hot return air carrying the heat generated by the servers via water to the *cooling towers* located outside of the DC building. Then, the heat is dissipated into the ambient by using large fans to blow the outside air through the cooling towers. If the temperature of the outside is not low enough to remove the entire heat and produce the return water with a desired temperature setpoint (e.g., 6°C), *water chillers* are used to remove the remaining heat and reduce the temperature of the water to the setpoint. Differently, the air-side economizer uses fans to inhale the outside air directly into the server rooms and blow out the hot air into the ambient. The DCs often adopt a hybrid of the air-side economizer and the traditional cooling equipment (e.g., the compressor-based air conditioners). When the outside air temperature is high, the conditioners are activated to cool the air before being supplied to the server rooms. In general, the air-side economizers can achieve higher energy efficiency than the water-side economizers for the DC cooling systems [9].

In our project, we focus on investigating the feasibility of the air-side economizers (referred to as air free-cooling) in the tropics. Table 1 summarizes the methodology and objective of our project and existing works [8]–[14] that studied the feasibility of the air free-cooling in various climates. These existing works can be divided into the following two categories. The first category [8]–[12] investigated energy efficiency of the air free-cooling based on the analysis of the historical weather data and/or simulations. The second category [13], [14] implemented and experimented with real container/modular DC testbeds. These works mainly focused on investigating the energy usage of the testbed. As presented in Table 1, in addition to the energy efficiency, our work also evaluates the server performance and hardware reliability under various air free-cooling settings on a real testbed. Moreover, we conduct analysis to investigate the solutions that can deal with several issues in operating the supporting facilities of air free-cooled DCs.

2.2 Impact of DC Environment Condition on Server Reliability and Performance

Temperature and RH are generally thought to have significant impact on the server hardware's reliability and computing performance. Existing works [20]–[24] have studied the impact of temperature. Their results show that the relationship between the failure rate of server components (e.g.,

1. PUE is the ratio of the total infrastructure power to the IT equipment power. A higher PUE value means that the data center is less energy-efficient.

2. Publicly available at <https://bit.ly/31sWPKS>, DR-NTU.

3. All appendices of this paper can be found in the supplementary file.

TABLE 1: Summary of existing studies on feasibility of air free cooling.

| Studies | Location | Methodology | | Objective | |
|--------------------------------|-------------|---------------------|--------------|-------------------|--------------|
| | | Simulation/Analysis | Real testbed | Energy Efficiency | IT equipment |
| Green Grid [8] | Worldwide | ✓ | - | ✓ | - |
| Khalaj <i>et al.</i> [9] | Australia | ✓ | - | ✓ | - |
| Ham <i>et al.</i> [10] | South Korea | ✓ | - | ✓ | - |
| Udagawa <i>et al.</i> [11] | Japan | ✓ | - | ✓ | - |
| Depoorter <i>et al.</i> [12] | Europe | ✓ | - | ✓ | - |
| Siriwardana <i>et al.</i> [13] | Singapore | - | ✓ | ✓ | - |
| Endo <i>et al.</i> [14] | Japan | - | ✓ | ✓ | - |
| Our study | Singapore | ✓ | ✓ | ✓ | ✓ |

HDD and memory) and the temperature appears to be sub-exponential or polynomial. In addition, high temperatures may negatively affect the server's performance, i.e., server's computing throughput and power usage. Furthermore, the existing studies [25], [26] have shown that with clean air, the RH has little impact on the server hardware reliability. Thus, modern servers can operate reliably under high RHs (e.g., 85% with ASHRAE's Class A3 servers) in typical DCs, in which the supply air is filtrated and recirculated within the enclosed DC buildings. However, a recent study by Manousakis *et al.* [22] based on the data collected from a number of Microsoft air free-cooled DCs found that the RH has dominant impact on the server component failures. Moreover, the studies [25], [26] reported that in the presence of the air-borne corrosive gases (e.g., SO₂, H₂S and NO₂) and particulate contaminations, the high RH can lead to increased server hardware failure probability. The reason is that when the RH of the supply air is high, the air particles and gases will absorb the air moisture to form corrosive pastes and acids that promote corrosion on printed circuit boards (PCBs) [27]. Given the PCBs' dense layouts today, the corrosion can easily cause short circuits and damage.

However, these works mostly relied on the data collected from production DCs with standard and stable environment conditions. Therefore, their observations may not capture the impact of all possible environment conditions under the free cooling in the tropics. Differently, our work builds a real air free-cooled DC testbed and conducts experiments to capture long-term impacts of many factors on the server reliability and computing performance.

3 DESIGN AND CONSTRUCTION OF TESTBED

This section describes the design of the testbed and our experiences in constructing and configuring the testbed.

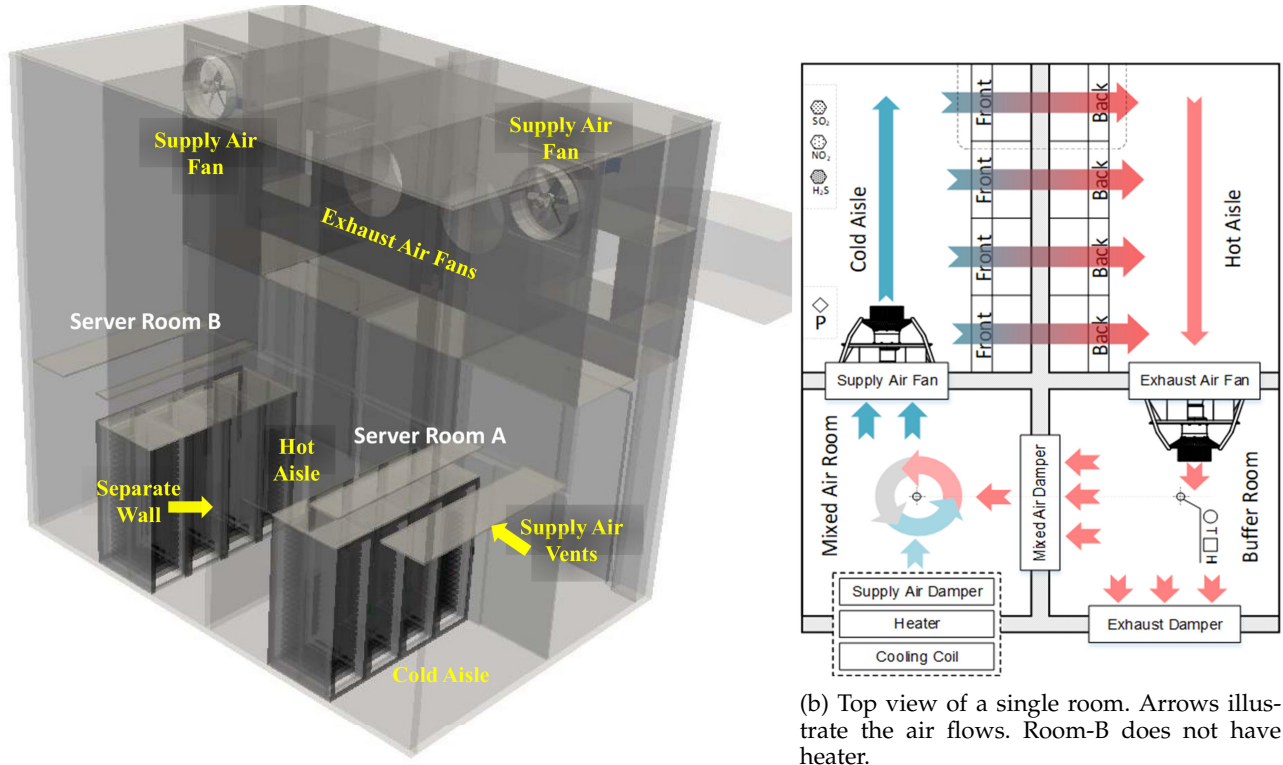
3.1 Design of Testbed

A committee consisting of researchers and practitioners is appointed to design the testbed. There are three design objectives. First, on the testbed, we can maintain the condition of the air supplied to the IT equipment at a certain setpoint for a period of time (e.g., several days). The condition includes temperature, RH, and air flow rate that are often considered important for IT equipment performance and reliability. The setpoint can be adjusted within a wide range, such that we can evaluate the performance of the IT equipment under various conditions. In other words, we can run

the testbed in a *controlled* mode. However, we later found that RH control in a wide range is difficult, which will be discussed with more details in Section 4.2.2. Thus, we focus on controlling the temperature and air flow rate. Second, we can run the testbed in an *uncontrolled* mode, in that we just use the outside air without adjusting its condition to take away the heat generated by the IT equipment. We aim to run the testbed in this uncontrolled mode for an extended period of time to understand the direct impact of the outside air on the IT equipment and the achievable energy saving. Third, the testbed should include a standard server room with controlled conditions to generate the baseline results.

To meet the above three objectives, we design a testbed consisting of three server rooms that are referred to as Room-A, Room-B, and Room-C in this paper. Fig. 1(a) shows the design of Room-A and Room-B. To support the aforementioned controlled and uncontrolled experiments, Room-A and Room-B are two side-by-side purposely built server rooms as shown in Fig. 2(c). The side-by-side arrangement makes sure that they will inhale outside air with the same condition, enabling comparative experiments. We built these two server rooms in the premise of a commercial colocation DC operator that is referred to as Operator-A in this paper. As such, we may leverage the domain expertise of Operator-A in facility management, 24/7 monitoring, security assurance, emergency response, and etc. Room-C is a standard server room operated by another commercial colocation DC operator that is referred to as Operator-B.

Fig. 1(b) shows the top view of a single server room (Room-A or Room-B). As shown in Fig. 1(b), Room-A has a cooling coil and a heater to maintain the supply air temperature. It has two fans, i.e., supply air fan and exhaust air fan, to move the air. In addition, it has three air dampers, i.e., supply air damper, exhaust damper, and air mixing damper. By setting the openness of the three dampers, we can control the percentage of the hot air generated by the IT equipment that will be mixed with the cold, relatively humid outside air to form warm, relatively dry air for the IT equipment. This design gives a certain level of RH control capability that can be used to reduce the negative impact of airborne contaminants on the reliability of the IT equipment. The difference between Room-B and Room-A is that, Room-B does not have a heater. This reduces the equipment cost and does not impede our experiments, because we can assign the controlled experiments with high temperature setpoints to Room-A.



(a) 3D view of Room-A and Room-B.

(b) Top view of a single room. Arrows illustrate the air flows. Room-B does not have heater.

Fig. 1: Design of Room-A/B.

We engaged a industrial partner to build a computational fluid dynamics (CFD) model and perform simulations to verify whether the testbed design can be meet our requirements. Specifically, the CFD model was built by a domain expert using a k-epsilon model with a mesh size of 937,723. Examples of simulated temperature and air flow velocity distributions in Room-A can be found in Fig. 2 in Appendix D. During the CFD simulations, the partner adjusted the server room layout design and the choice of the cooling equipment until all design requirements are satisfied. Then, the testbed was constructed based on the design specifications verified with the CFD simulations. After the testbed was commissioned, the partner used the measurements collected from the testbed to evaluate the accuracy of the built CFD model. The evaluation shows that the CFD model achieves a root mean square error (RMSE) of 1.2°C in predicting temperatures in the server rooms. Note that we did not perform CFD simulations in the experiment phase of our project. In this paper, all results and observations were drawn from our real testbed experiments.

Room-C follows the typical raised floor design and has a computer room air conditioning (CRAC) unit. We purposely improved its energy efficiency to make it an optimistic baseline by adding a cold air containment design. Illustration of the layout of Room-C with an air containment and the air flows can be found at Fig. 3 in Appendix D.

3.2 Construction of Testbed

The construction of Room-A/B undertaken by a contractor took about four months. Fig. 2(a) shows the two side-by-

TABLE 2: Description of deployed sensors.

| Sensor | Qty | Location | Accuracy |
|------------------|-----|-----------------|---------------------|
| Temperature | 1 | outdoor | ±0.3°C |
| RH | 1 | outdoor | ±3% |
| Temperature | 4 | chambers | ±0.3°C |
| Air velocity | 4 | cold vents | ±1m/s |
| Air pressure | 1 | cold aisle | ±0.8% |
| SO ₂ | 1 | cold aisle | ±5% |
| NO ₂ | 1 | cold aisle | N/A* |
| H ₂ S | 1 | cold aisle | ±3% |
| PM2.5 | 1 | cold aisle | ±1µg/m ³ |
| Temperature | 24 | 6 for each rack | ±0.3°C |
| RH | 24 | 6 for each rack | ±3% |
| Air pressure | 12 | 3 for each rack | ±0.8% |
| Power | 8 | 2 for each rack | Class 1 |
| Power | 4 | in facility | Class 1 |

*Calibrate at every 6 months for accuracy

side storage rooms located within the premise of Operator-A that were later retrofitted into Room-A and Room-B. Figs. 2(b) and (c) show the exterior of Room-A and Room-B during and after the construction, respectively. As seen in Fig. 2(c), two supply air ducts were constructed such that there is sufficient space separation between the air inhaled and exhausted by Room-A/B. Passive air filters of Class MERV-6 were installed in the air ducts to prevent PM10 and larger particles from entering the server rooms. These passive filters do not use energy. The red pipelines shown in Fig. 2(c) belong to a fire protection system. Fig. 2(d) shows

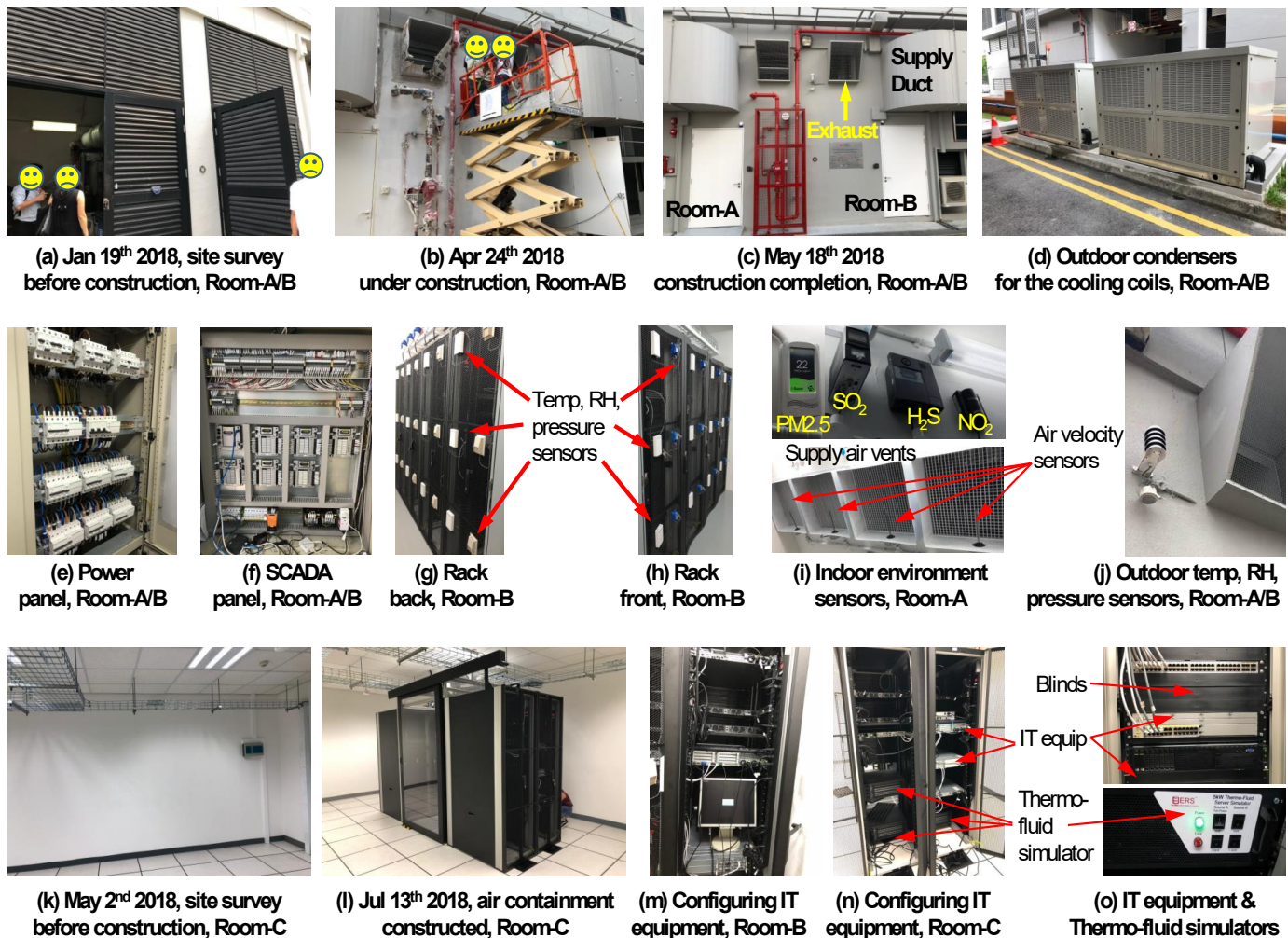


Fig. 2: Construction and configuration of Room-A, Room-B, and Room-C of the testbed.

the outdoor condensers for the cooling coils installed in Room-A/B. The distance from these condensers to Room-A/B is about 30 meters to reduce the heat recirculation from the condensers to the two rooms. Fig. 2(k) shows an empty server room provided by Operator-B to be retrofitted as Room-C. Fig. 2(l) shows the four racks that we deployed in Room-C with the constructed cold air containment.

Table 2 summarizes the quantities and locations of the sensors deployed in our testbed. We install a total of 87 sensors in various modalities to monitor the real-time environmental condition of the test rooms and the power consumption of the IT equipment and room facility. Figs. 2(g)-(j) show various sensors deployed in Room-A and Room-B. All sensors deployed in Room-A/B are Supervisory Control and Data Acquisition (SCADA) slaves communicating with a SCADA master using Modbus TCP protocol. Figs. 2(e) and (f) show the power and SCADA panels for Room-A/B.

In each server room, we deployed four 42U IT racks. Thus, our testbed of three rooms hosts a total of 12 racks. The planned power rating for each rack is 5 kW. If all racks are fully populated with servers, the capital expenditure (Capex) for IT equipment will be twice of the Capex for constructing all the supporting facilities shown in Fig. 2. We received a total of 33 on-loan IT devices from four major IT equipment manufacturers. We deployed the same set of 11

IT devices in each server room, as shown in Figs. 2(n) and (o). As the racks are not fully populated, to increase cooling efficiency, we applied blinds as shown in Fig. 2(o) on the empty rack slots. Moreover, to increase the power usage of the IT racks for realism of the experiments, we deployed four in-rack thermo-fluid simulators in each of Room-A and Room-B, and eight in Room-C, as shown in Fig. 2(n). The thermo-fluid simulator can be configured manually to use a certain power among multiple discrete levels up to 5 kW. With the thermo-fluid simulators, we can reduce the Capex of the testbed, while maintaining its realism in terms of power usage and heat generation. Thanks to Operator-A's and Operator-B's provision of the spaces, the operating expenditure (Opex) of the testbed is mainly the electricity cost. The Opex of operating the testbed over about 1.5 years is about 10% of the Capex for constructing the testbed.

3.3 Configuration of Testbed

We configured all servers and network switches/routers so that we can easily control their operations for experiments. Moreover, as all the three server rooms are located in the premises of Operator-A and Operator-B, it is desirable that we can access all IT equipment and the supporting facilities remotely from our university campus. The remote access

| Room-A | Room-B | Room-C |
|---|--|--|
| System check (2 weeks) | | |
| Controlled CPU test (2 months) | | |
| Controlled HDD test (2 months) | | |
| Controlled memory test (2 months) | | |
| Controlled node test (2 months) | | |
| Uncontrolled test: Fixed air volume flow rate (8 months) | Uncontrolled test: Adaptive air volume flow rate (8 months) | Controlled node test with raised temperature and IT load (8 months) |

Fig. 3: The experiment plan.

should be configured prudently with cybersecurity in the mind. Although the IT equipment on the testbed will not be used for production, we have a major concern regarding cyber-attacks that take over the SCADA system to damage the costly supporting facilities and/or use the facilities to create safety incidents (e.g., fires by the heater).

We installed the unmodified CentOS v6.9 GNU/Linux on all the servers and configured the switches to form an Intranet in a fat tree topology. We configured three routers on our testbed to use three public IPv4 addresses. Once we made our routers publicly accessible, we observed multiple rounds of port scanning from the Internet, which is often the first step of cyber-attacks. We applied a whitelist of accessible ports and remote host IP addresses to restrict the access. The SCADA master provides a password-protected web interface to access real-time or historical sensor data and adjust the setpoints of actuators (heater, supply/exhaust fans, air dampers, and cooling coils). The SCADA master was configured to use HTTPS protocol for the web interface to ensure the integrity and confidentiality of the communications between the testbed and our campus.

We developed a set of BASH scripts to control and monitor the servers' running status. (1) For CPU status control, we use `cpulimit` v0.2 to maintain the utilization of each physical core of a CPU at a specified level. Then, we use a customized `LINPACK` benchmark provided by the CPU vendor to measure the CPU performance. (2) For HDD status control, we use the `cgroups` to maintain the read/write throughput of the HDDs configured to operate in the RAID0 mode. Then, we use `fiio` to generate HDD read/write requests. (3) For memory status control, we use `mementester` to generate test traffic and find memory faults. (4) For server status monitoring, we use various tools such as `cpupower`, `imptool`, and `lm_sensor`. The collected data traces are uploaded periodically to Google Cloud Storage. During the combined tests of all the scripts we developed, we found that when we tried to maintain the CPU utilization at 100%, IMPI's sampling experienced significant jitters, degrading the quality of the server status monitoring. Thus, in our planned experiments (cf. Section 4.1), the highest CPU utilization to be maintained for extended period of time was 90%. We only conducted short-period experiments for 100% CPU utilization.

Our industrial partner implemented the following algorithms for the air volume flow rate and temperature controls. First, the partner implemented a proportional-

integral-derivative (PID) controller for adjusting rotating speeds of the supply and exhaust fans to maintain the air volume flow rate at a desired setpoint. At every two seconds, the controller takes the total air volume flow rate measured by the air velocity sensors as feedback to adjust the fan speed such that the difference between the setpoint and the measured air flow rate is minimized. The control error is within 5%. Second, a bang-bang controller for the cooling coil and heater was implemented to maintain the supply air temperature at a desired setpoint. The cooling coil/heater has several setpoints, each of which provides a specific cooling/heating capacity. Regardless of dynamics of the outside air temperature, at every two seconds, the controller reads the temperature sensors installed at the middle heights on the front of IT racks. Then, it adjusts the setpoint of the cooling coil/heater to minimize the difference between average of the measurements and the temperature setpoint. The error temperature is about 1°C.

In the planned experiments (cf. Section 4.1), the operations of the tested servers and the supporting facility need to be coordinated. Thus, we configured the NTP clients on the tested servers and the SCADA master of our testbed to synchronize their clocks with Singapore's local pool of NTP servers. The second-accurate clock synchronization of NTP over Internet suffices for the needed coordination.

4 EXPERIMENTS ON THE TESTBED

In this section, we present the design of experiments (Section 4.1), experiences and results of the experiments conducted with the facilities (Section 4.2) and IT equipment (Section 4.3).

4.1 Design of Experiments

We conducted the following two groups of experiments: controlled tests and uncontrolled tests. Fig. 3 shows the planned experiments. The time periods shown in Fig. 3 are net test times. From our experience, there were also various overheads that consumed the project time, such as repair of faulty devices, additional tests to verify results, and facility maintenance. We planned to complete all tests shown in Fig. 3 in a duration of 20 months.

4.1.1 Controlled tests

A controlled test focuses on a key component of the server, i.e., CPU, HDD, and memory. Specifically, during a *unit test* of a controlled test, the ambient condition (temperature and air volume flow rate) and the operating status of the tested component are maintained at a certain level for one hour. A controlled test consists of hundreds of unit tests with all combinations of the server room ambient condition and server component status each sweeping the respective range summarized in Table 3. Note that the maximum temperature setpoint of 37°C is the record maximum ambient temperature in Singapore. During the controlled node test, we simultaneously vary the operating status of CPU, HDD, and memory. For the first four controlled tests in Room-C, the temperature setpoint for the return hot air is set to be 20°C as suggested by Operator-B. The CRAC unit controls the volume flow rate of the cold air supplied to the four

TABLE 3: Experiment settings for controlled experiments.

| Parameters | Min | Max | Step |
|------------------------------------|-------------------------|-------|------|
| Supply air temperature | 25°C | 37°C | 1°C |
| Air flow rate* (m ³ /h) | 2500 | 12500 | 2500 |
| CPU utilization (%) | 10 | 90 | 20 |
| HDD speed (MB/sec) | 10 | 100 | 20 |
| Memory block size (kB) | 8, 16, 32, 64, 128, 256 | | |

*Applicable for Room-A and Room-B.

racks. In the last controlled test in Room-C, we vary the temperature setpoint from 21°C to 35°C with step size of 1°C and the total power of eight thermo-fluid simulators within [10 kW, 20 kW, 30 kW, 35 kW]. The controlled tests allow us to understand the performance and thermal safety of the IT equipment under various conditions. During a unit of the controlled tests, the steady state of the experiments includes the supply air temperature, the air volume flow rate, and the server’s operating parameters (i.e., CPU utilization, HDD speed and memory block size).

4.1.2 Uncontrolled tests

We designed two uncontrolled tests, namely fixed and adaptive ventilation, in Room-A and Room-B, respectively, in which the fans are used to inhale the outside air into the server rooms. The air entering the server room is not conditioned by cooling coils and heater. Thus, the servers experience the ambient temperature and RH directly. These uncontrolled tests allow us to assess the energy savings achieved by the air free-cooling design that purely uses the outside air for cooling in Singapore’s tropical condition. Modern DCs often adopt a hybrid cooling scheme [28] which combines the air free-cooling with the traditional cooling approach to control the supply air condition. Specifically, when the outside air temperature is higher than the temperature setpoint, the cooled air from the traditional cooling system is mixed with the outside air to maintain the supply air temperature at the setpoint. Although the testbed maintains the supply temperature at certain setpoints in the first phase (i.e., controlled tests) of our project, the objective is not to save energy. Instead, the main objective of the first phase is to test whether the servers can sustain under various supply air temperatures up to 37°C (i.e., the maximum record temperature in Singapore). Because our experimental results show that the temperature up to 37°C has no/little impact on the server’s computing performance and reliability, we can use the air free cooling for 100% of time without the concern of server overheating. Thus, we do not study the hybrid cooling approach in our project.

Table 4 summarizes the settings for the uncontrolled tests. Specifically, in the uncontrolled tests, the supply air temperature is close to the outside air temperature which varies over time. The server’s operating parameters are maintained at the constant values. With the fixed ventilation, the air volume flow rate is fixed at 5000m³/h. Thus, the steady state of the experiments with the fixed ventilation includes the air volume flow rate and the server’s operating parameters. On the other hand, with the adaptive ventilation, the steady state of the experiments consists of the server’s operating parameters, because we adapt the air

TABLE 4: Experiment settings for uncontrolled experiments.

| Parameters | Fixed | Adaptive |
|-----------------------------------|---------|--------------|
| Supply air temperature | Outside | Outside |
| Air flow rate (m ³ /h) | 5000 | [200, 12500] |
| CPU utilization (%) | 100 | 100 |
| HDD speed (MB/sec) | 100 | 100 |
| Memory block size (kB) | 256 | 256 |

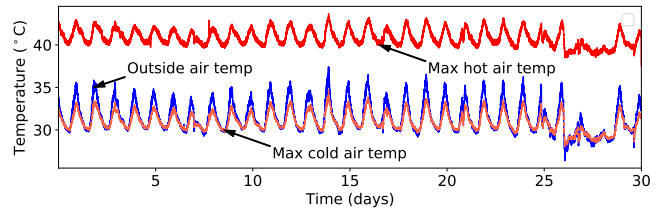


Fig. 4: Air condition under fixed ventilation for 30 days of August 2019 in Room-A. The room air volume flow rate is fixed at 5000 m³/h. The “max cold air temp” and “max hot air temp” curves show the traces of the maximum among all the cold and hot air temperatures measured by temperature sensors deployed at four IT racks over time, respectively.

volume flow rate in response to change of the outside air temperature.

To avoid the damages to the server components, most servers will automatically shutdown when their inlet temperature exceeds a safety threshold. For continuous operation of a DC, the maximum temperature of the all server’s inlets should be always maintained below the safety threshold. The test results obtained in our controlled tests show that the minimum value of tested supply air volume flow rate setpoint (i.e., 2500 m³/h) can ensure no server shutdown and overheating on the IT racks even under the most extreme condition (i.e., 37°C and full utilization of servers). However, to maintain a safety margin, we set the fixed air volume flow rate to 5000 m³/h in the uncontrolled tests with the fixed ventilation in Room-A. Fig. 4 shows 30 days’ traces of outside air temperature, maximum among cold and hot temperatures measured temperature sensors deployed at three heights on the front and back sides of four IT racks, respectively, under the fixed ventilation tests. During the test period of 30 days, the maximum cold air temperature is close to the outside temperature whose maximum value is less than 37°C. The maximum hot air temperature is always lower than 44°C in the 30-days period. Note that most of servers deployed in our testbed have a safety threshold of 45°C for the server’s inlet temperature. Thus, these results imply that under the fixed air flow rate of 5000 m³/h, the server’s inlets is thermally safe during the test period. Moreover, the maximum cold air temperature is about 8°C lower than the server’s safety threshold of 45°C.

In the adaptive ventilation test in Room-B, we implemented a control logic that adjusts the supply air flow rate f_s by controlling the room fan speed such that the maximum air temperature measured by the temperature sensors installed on the IT racks’ back sides at the hot aisle is always maintained below a temperature threshold of t_{th} . Fig. 5 illustrates the control logic of the adaptive ventilation.

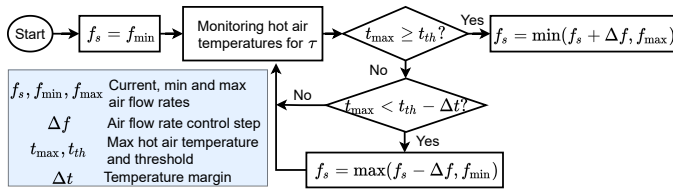


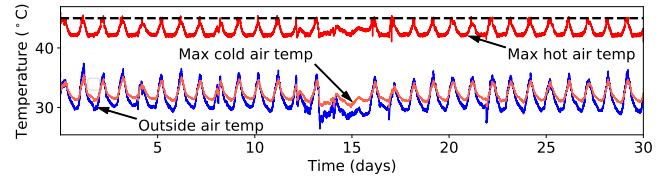
Fig. 5: Control logic of the adaptive ventilation.

Specifically, the adaptive ventilation test initially adopts the minimum setpoint of f_{\min} for the supply air volume flow rate. Then, the f_s is adjusted at every control period of τ . At the beginning of the period τ , if the maximum hot air temperature t_{\max} at the hot aisle is equal to or higher than the t_{th} , the f_s is increased by a control step of Δf unless the f_s already reaches the maximum air volume flow rate, denoted by f_{\max} that the ventilation system of the testbed can provide. Otherwise, if the $t_{\max} < t_{th} + \Delta t$, where $\Delta t > 0$, the f_s is decreased by Δf . Note that the server's inlet temperature is always less than the temperature of the hot air that carries the heat generated by the servers. Therefore, to maintain a thermal safety margin, the control logic considers the maximum hot air temperature as the control objective, instead of the server's inlet temperature.

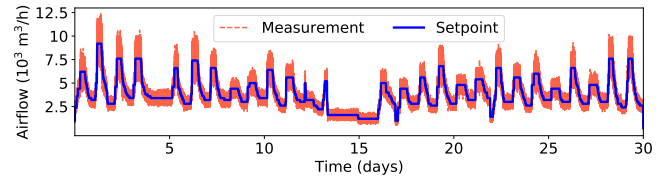
In our adaptive ventilation tests, we used the following settings: $t_{th} = 45^\circ\text{C}$, $\tau = 1$ minute, $f_{\min} = 200\text{ m}^3/\text{h}$, $f_{\max} = 12500\text{ m}^3/\text{h}$, $\Delta f = 200\text{ m}^3/\text{h}$, and $\Delta t = 3^\circ\text{C}$. Fig. 6 shows the air volume rate, maximum cold and hot air temperatures across temperature sensors deployed at the front and back sides of the four IT racks, respectively, during 30 days under the adaptive ventilation test. Note that in Fig. 6(b), there are two curves corresponding to the air volume flow rate setpoint and measurement. The setpoint is the output of the control logic. Given the required setpoint, the measurement is the actual volume flow rate taken by the sensors. From Fig. 6, we can see that the adaptive ventilation can adapt the air volume flow rate in response to the change of the outside temperature and maintain the maximum hot air temperature below the targeted threshold. The maximum cold temperature is lower than the server's safety threshold of 45°C by a margin of about 8°C . Moreover, the average of the air volume flow rate measurements over the test 30-day test period is about $3800\text{ m}^3/\text{h}$. These results imply that the adaptive ventilation can reduce the energy used by the fans, compared with the fixed ventilation approach. This is because the adaptive ventilation adapts the fan speed in response to the variation of the outside air temperature such that a right enough amount of the outside air is blown into the server room while maintaining a similar safety margin for the server. Specifically, when the outside air temperature is low, with the adaptive ventilation, the fans can rotate at a low speed. As such, the total fan energy usage can be reduced.

4.2 Experiments with Facilities

In this section, we discuss several important issues in operating the supporting facilities and the key measurement results.



(a) Air temperatures. The horizontal dash line represents a temperature threshold $t_{th} = 45^\circ\text{C}$



(b) Room air volume flow rate.

Fig. 6: Air temperature and volume flow rate condition under the adaptive ventilation for 30 days of August 2019 in Room-B.

4.2.1 Dew point prevention

During the controlled experiments, the cooling coils are used to maintain the cold aisle temperature at the setpoint. When the outside air is hot and humid (e.g., before an afternoon rainfall), the temperature of the cooled air leaving the cooling coil may reach the dew point. In fact, we did see drained water from the cooling coil, which is an indication of 100% RH for the cooled air. As such, the saturated cold air may condense on a colder surface. If such condensation occurs on the PCBs of the IT equipment, the resulted short circuits may damage the IT equipment. This concern can be mitigated by the fact that the heat generated by the IT equipment increases the temperature and thus decreases the RH of the air passing through the IT equipment. For the safety of the servers, we implemented a dew point prevention mechanism in the control algorithms for the cooling coils. Specifically, if the temperature setpoint is more than 3°C lower than the outside air dew point, we stop conditioning the inhaled air. Fig. 7(a) shows the outside temperature and dew point during July and October 2018 in the testbed area. We can see that the dew point fluctuates at around 25°C , which is the minimum temperature setpoint during our controlled tests. Thus, this dew point prevention mechanism disallowed the tests with low temperature setpoints for limited time duration. With this mechanism and the heat generated by the IT equipment, the RH at the cold aisle is capped at 90%. We would like to stress that the dew point prevention must be considered for any air free-cooled DCs, especially in the areas with high RH levels.

4.2.2 Cooling-then-mixing approach

As mentioned in Section 3, the original design objectives of our testbed include RH control capability. However, from the discussions with facility suppliers and our study, we found that for Room-A and Room-B, implementing RH setpoints in a wide range under Singapore's tropical condition is costly and technically challenging. Specifically, as Room-A and Room-B continuously inhale the outside air, the commercially available dehumidifier and humidifier

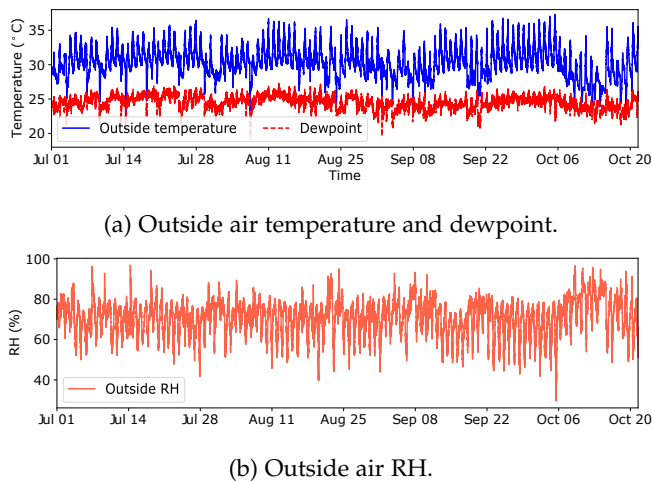


Fig. 7: Outside air condition during Jul and Oct 2018 in the testbed area.

consume a large amount of energy for the RH control under air flow rate setpoints up to $12500 \text{ m}^3/\text{h}$ in our experiment plan. Therefore, we decided to not install the dehumidifiers and humidifiers for the RH control in the testbed. Note that typical DCs often have enclosed environment, in that the air is circulated within the DC building. As they inhale a limited amount of air from the outside, they have low dehumidification and humidification demands. Then, we studied a possible energy-efficient *cooling-then-mixing* approach which can be used to maintain specific supply air temperature and RH setpoints, given the condition of the outside air, cooling capacity of the cooling coil and total IT power. Specifically, to maintain a desired supply air RH setpoint different from the outside air RH, this approach firstly uses a cooling coil to condense and remove the water vapor contained in the outside air entering the server room. Then, the dried air is mixed with a controlled portion of the recirculated hot air to maintain the desired setpoint for supply air temperature.

Now, we model the cooling-then-mixing process to study its feasibility in maintaining specific temperature and RH levels under Singapore's tropical condition. We define the following notation: t_o and ϕ_o are temperature and RH of the outside air entering the server room, t_s and ϕ_s are temperature and RH of the mixing air supplied the servers, f_s is supply air volume flow rate, $q_c \geq 0$ is cooling capacity of the cooling coil, α is controlled fraction of the hot air in the supply air, and p_{IT} is total power of the IT equipment. We have derived a psychrometric model to determine the supply air condition as follow:

$$t_s, \phi_s = f(t_o, \phi_o, f_s, q_c, p_{IT}, \alpha), \quad (1)$$

where $f(\cdot)$ includes mass and energy conservation equations which characterize the psychrometrics of air heating, cooling and mixing processes in the cooling-then-mixing approach. The detailed forms of these equations can be found in Appendix B.

The derived model takes the outside temperature t_o and RH ϕ_o , cooling capacity q_c , IT power p_{IT} and fraction of the recirculated hot air α as inputs to determine the supply air

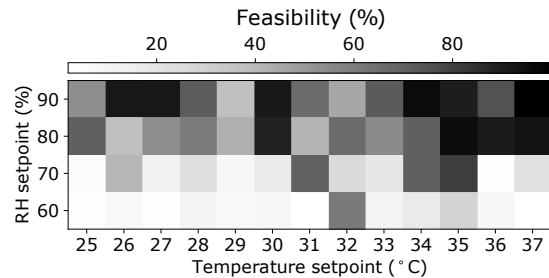


Fig. 8: Feasibility of temperature/RH setpoints during Jul to Oct 2018 in the Singapore's testbed area.

temperature t_s and RH ϕ_s . We use the model to assess the ability of the cooling-then-mixing approach to maintain the t_s and RH ϕ_s at specified setpoints. Specifically, given the t_o , ϕ_o and p_{IT} , we search the f_s , p_c and α within their ranges of $[2500 \text{ m}^3/\text{h}, 12500 \text{ m}^3/\text{h}]$, $[0, q_{\max}]$ and $[0, 1]$, to ensure that the t_s and ϕ_s equals to the specified setpoints. Note that q_{\max} is the maximum cooling capacity of the cooling coil. Given the t_o , ϕ_o and p_{IT} , the t_s , ϕ_s are considered infeasible if no such f_s , p_c and α are found.

The grayscale in Fig. 8 shows the percentage of time from July to October 2018 in our testbed area during which the corresponding supply air temperature t_s and RH ϕ_s setpoints on the x -axis and y -axis, respectively, can be maintained by the cooling-then-mixing approach, given the outside air condition as shown in Fig. 7. The p_{\max} and p_{IT} are set to the testbed's maximum cooling capacity of 200 kW and IT power of 20 kW, respectively. From Fig. 8, we can see that it is difficult to maintain low temperature and RH setpoints simultaneously for long periods of time. In other words, the cooling-then-mixing approach does not allow us to perform the test under wide ranges of temperature and RH levels, given the Singapore's tropical weather condition. Specifically, we may hardly maintain the supply air temperature below 37°C and RH below 65% using this approach. Note that 65% is a critical RH threshold related to server reliability, which will be further explained in Section 5. In summary, the RH control based on the humidifiers and/or dehumidifiers would incur high energy usage in the testbed. The above cooling-then-mixing approach is incapable of RH control in wide ranges for experimentation. Therefore, we did not apply RH control for this testbed. This is a limitation of our testbed and calls for further research in the future.

The cooling-then-mixing approach is incapable of maintaining wide ranges of temperature and RH setpoints for our planned experiments. However, our previous research [29] shows that if the IT equipment can tolerate a supply air temperature of 45°C , this approach can largely maintain the RH below 65% in Singapore's condition. Note that ASHRAE Class A4 IT devices that can tolerate 45°C supply air are increasingly available. Moreover, this approach in general has high energy efficiency. Specifically, with the high temperature and RH setpoints, the air condensation by the cooling coil may not be always active. Mixing the outside air with the recirculated hot air can maintain the supply air temperature and RH at the setpoints. In our testbed, the hot air recirculation is implemented and controlled by the air mixing damper as shown in Fig. 1b. From our measurements, the energy usage of the damper is little, compared

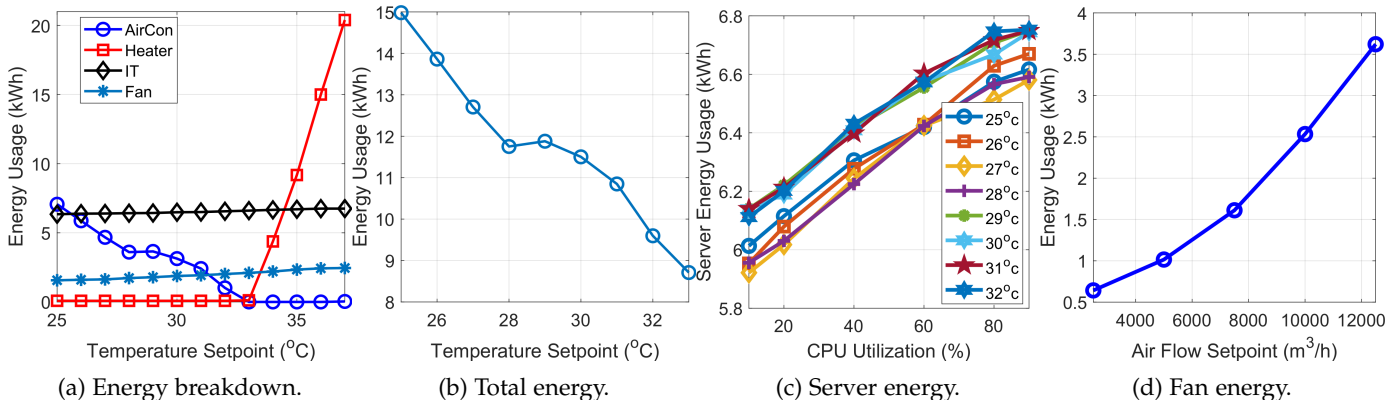


Fig. 9: Energy profile of Room-A. The measurements in (a) and (b) were collected during a 13-hour experiment.

with that of other cooling equipment, including the room fans and cooling coils. Therefore, the cooling-then-mixing approach based on our design shown in Fig. 1(a) is promising to operate the air free-cooled tropical DC in Singapore, especially when the high temperature and relatively low RH setpoints are adopted. However, under this approach, precise control is non-trivial since the air free-cooled DCs in general operate in the presence of exogenous disturbances, including the time-varying outside air condition and dynamic IT workload. This calls for further research to study the feasibility of the precise temperature and RH control. The advanced deep reinforcement learning (DRL)-based control algorithms [29] can be adopted to achieve the goal. Specifically, we can use the CFD model (cf. 3.1) to generate extensive data to train a neural-network-based digital twin of the testbed. Then, the trained digital twin can be used as a DC simulation platform to evaluate DRL-based control algorithms.

4.2.3 Energy profiles

We conducted a set of experiments to understand the energy usage profile of Room-A/B. Fig. 9(a) shows the energy usage of cooling coil, heater, and server racks in Room-A when the temperature setpoint was varied from 25°C to 37°C during a 13-hour experiment. Each data point in the figure is the energy usage during one hour. When the temperature setpoint was greater than 33°C, the outside temperature was lower than the setpoint. Thus, the cooling coil stopped working and the heater started operation. The energy usage of the server racks increased by 6% when the temperature setpoint was varied from 25°C to 37°C. This is because the server enclosure’s built-in fans rotate faster when the inlet temperature increases. Fig. 9(b) shows the total energy drop of Room-A by about 45% when the temperature setpoint was increased from 25°C to 33°C. This suggests that a significant energy saving can be achieved by air free-cooling. The curve in Fig. 9(b) raises when the temperature setpoint is greater than 29°C. This is because there was an outside temperature increase after we completed the test with the temperature setpoint of 28°C.

Fig. 9(c) shows the total server energy usage in Room-A when the CPU utilization was varied from 10% to 90% and the temperature setpoint was increased from 25°C to 32°C. Each point is the energy measurement over one hour. We can see that, although the server energy in general increases

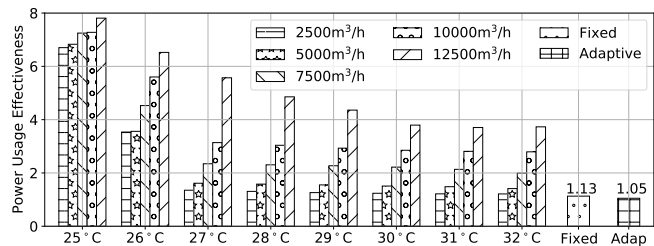


Fig. 10: PUEs in controlled and uncontrolled tests. (The results with specified temperature and air volume flow rate setpoints are from the controlled tests; the results labeled “Adaptive” and “Fixed” are from the uncontrolled tests.

with the temperature setpoint due to the faster server fan rotation, CPU utilization is a major factor affecting the server energy in a linear manner.

Fig. 9(d) shows the energy usage of the fans in Room-A when the temperature setpoint was fixed at 26°C and the air volume flow rate setpoint was increased from 2500 to 12500 m³/h. The fans used 5.4% to 22.6% of the total energy usage of Room-A. Our controlled experiments over eight months show that a volume flow rate of 5000 m³/h suffices for each of Room-A and Room-B to prevent overheating.

Fig. 10 shows that PUEs of controlled and uncontrolled tests. Specifically, we installed multiple power meters to measure the real-time power usage of IT racks, cooling devices (i.e., room fans, cooling coil and heater) and supporting facilities (e.g., lighting and fire protection system) at every five seconds. Let p_{IT}^i , p_c^i and p_s^i denote the total power of all IT racks, the total power of all cooling devices, and the total power of supporting facilities, respectively, at the i^{th} measurement time. We define N as a total number of samples of the power meter during the test period. The PUE is calculated as: $PUE = \sum_{i=1}^N (p_{IT}^i + p_c^i + p_s^i) / \sum_{i=1}^N p_{IT}^i$. Our PUE calculation is considered preferred among a number of calculation approaches proposed by The Green Grid [30].

Note that in the controlled tests, the heater is activated to maintain the temperature setpoint from 33°C to 37°C. The deployment of the heater is used for our tests only. Therefore, in Fig. 10, we present the PUEs of the controlled tests with the temperature setpoint lower than 32°C only. As shown in Fig. 10, the PUEs of the controlled tests are

TABLE 5: Summary of server performance tests.

| Tests | Tested component | | | Metrics |
|-------|------------------|-----|--------|------------------------|
| | CPU | HDD | Memory | |
| 1 | ✓ | - | - | GFLOPS, core frequency |
| 2 | - | ✓ | - | IOPS, response time |
| 3 | - | - | ✓ | Copying speed |
| 4 | ✓ | ✓ | ✓ | All |

GFLOPS: Figa floating point operations per second.

IOPS: input/output operations per second.

much higher than those of the uncontrolled tests since major energy is used by cooling coils and fans to maintain expected setpoints for the temperature and air flow rate. For instance, the PUE can be up to 7.81 when the temperature setpoint is 25°C and the air flow rate setpoint is 12500 m³/h. In the controlled tests, the PUE consistently decreases with the cold air temperature. On the other hand, the uncontrolled tests using only fans can greatly reduce the PUE. Specifically, the test with the adaptation ventilation logic for controlling the air flow rate illustrated in Fig. 5, can achieve a PUE of 1.05 as shown in Fig. 10. This implies that if the air free-cooling design is successful, the PUE can be reduced by 38%, compared to the global average PUE of 1.7 [15].

The lowest PUE of 1.05 that we achieved during the uncontrolled tests with the adaptive ventilation can be viewed as the lower limit of the PUE for air free-cooled setups. Thus, our experiments provide the baseline understanding of the achievable PUEs in the tropical area. Note that Facebook achieved an annualized PUE of 1.07 by air free-cooling in Oregon. Endo *et al.* [14] reported a PUE of 1.058 achieved by an air free-cooled DC testbed in Tokyo. We achieved a similar PUE in the Singapore’s tropical area.

4.3 Experiments with IT Equipment

This section presents the key results of the server computing performance and reliability from our tests.

4.3.1 Server performance

As discussed in Section 4.1.1, we conducted four sets of controlled tests to investigate the impacts of temperature and air volume rate setpoints on the performance of three server’s key components: CPU, HDD, and memory. Table 5 summarizes the methodology and measured performance metrics of these four tests. Our result analysis shows that the following operating conditions have little/no impact on the performance of the tested CPUs, HDDs and memories: (1) the temperature setpoint is from 25°C and 37°C and (2) the air volume flow rate is 2500 m³/h. Specifically, during the tests, all the tested CPUs were thermally safe and no core frequency throttling occurred. In other words, the tested servers can operate without computing performance degradation under a supply air temperature setpoint up to 37°C. The detailed description of the test results and analysis can be found in Appendix C. More details can be found in our technical report [31].

4.3.2 Component reliability

In all tests, we also measured various reliability data, such as correctable and un-correctable memory errors, HDDs’ latent



Fig. 11: Corrosion observed on the compact disk (CD) drive of a server in Room A. The rightmost figure shows the CD drive of the same model of server in Room C.

sector errors and self-monitoring, analysis, and reporting technology (SMART) records to investigate the reliability of the server’s components during the tests. The measurement results show that all tested HDDs and memories work successfully without any errors during the tests. Moreover, there are no overheating-induced server shutdowns when the aisle cold temperature setpoint is up to 37°C and the CPU is fully utilized. However, we observed several server faults on the testbed during the tests. These faults were not caused by the failures of the focus components (i.e., CPU, memory, and HDD). The detailed analysis of the faults will be presented in next section.

5 IT EQUIPMENT FAILURES

In this section, we summarize the IT equipment failures that occurred on the testbed during the tests. Then, we present our investigation on the reasons of the failures.

5.1 Summary of Failures

The testbed has a total of 18 servers from four different vendors which are deployed in three server rooms. During the tests, a number of servers in Room-A and Room-B had faults and could not be booted. Specifically, among 12 servers from the same Vendor 1 in Room A and Room B, six of them failed after about 6 months from the initial operation during the controlled tests. Vendor 1 performed on-site examination for the faulty servers. They found that the fan backplane of all failed servers and the motherboards of three servers malfunctioned. The CPU on one of the servers with the malfunctioned mainboard was damaged. Vendor 1 replaced the malfunctioned components to revive the servers. Then, after 6 months from the first repair, four of six fixed servers from Vendor 1 failed again during the uncontrolled tests. In addition, we encountered two server faults from Vendor 3 in Room A and Room B after 11 months from their initial operations. Severe corrosion can be observed on the compact disk drives of the two failed Vendor 3 servers, as shown in Fig. 11. Additional examples of corrosion and dusts resting on the PCBs of the motherboards of the faulty servers can be found in Figs. 4 and 5 in Appendix D. Note that all failures occurred on several servers from the same vendors. The remaining servers from other vendors and all network equipment, forming a large portion of all tested IT equipment, are still healthy after 18-month operation.

5.2 Investigation on Failure Reason

Vendors performed lab-based fault analysis on the faulty server components. We also investigated the server room

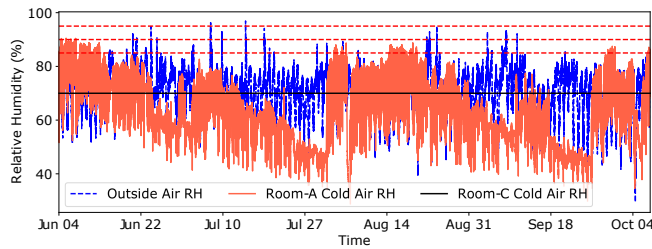


Fig. 12: RH of outside air, cold air in Room-A, and cold air in Room-C before the server faults in Room-A/B. The three horizontal dash lines represent the servers' maximum allowable RH levels specified in their datasheets.

condition to find the reasons of the server faults. In what follows, we provide detailed information of the vendors' fault analysis and our investigation.

5.2.1 Vendor's fault analysis

The vendor found that the faults of the mainboards and fan backplane were caused by dusts and/or corrosion on the PCBs. They used a microscope to examine the PCBs of the motherboards of the faulty servers. They can see dusts resting on the PCBs. The faulty motherboards functioned normally at room temperature in the lab. But the fault could be reproduced after liquid nitrogen was sprayed on the motherboard, suggesting that the fault was caused by dust. This is because when the moisture in the air condenses on the motherboard, the dust on the motherboard absorbs the condensed moisture and causes short circuits. After cleaning the motherboard using liquid, the motherboard restored and survived liquid nitrogen spray tests. The vendor also confirmed that high temperature is not the cause of the server failures. A faulty CPU is caused by the over voltage due to a failed power supply chip on the mainboard. In other words, the CPU failure is a cascading failure, which is not caused by overheating.

In summary, the vendor's fault analysis results show that (1) corrosion caused by airborne contaminants on the motherboards and other supporting PCBs is the main reason of the faults; (2) the server faults are not caused by CPUs, HDDs, and memories; and (3) high temperature is not a reason of the server faults.

5.2.2 Our investigation

We investigated the following aspects on the potential reasons of the server failures.

Temperature. The faulty servers are compliant with ASHRAE's A3 or A4 requirement, i.e., they can operate reliably under inlet temperature of 40°C or 45°C. As the maximum cold aisle temperature was 37°C during the tests, this double confirms that the high temperature is not the reason of the faults.

RH. From the servers' datasheets, each server requires that the RH is lower than a threshold among 85%, 90%, and 95%. Fig. 12 shows the traces of outside air RH and the cold air RH in Room-A during three months before the server faults occurred. Note that because we varied the cold air temperature in Room-A during the controlled experiments, the cold air RH changed accordingly as shown in Fig. 12. We

TABLE 6: A server vendor's requirement and our measurement.

| Gas | Required* (ppb) | Long-Term (ppb) | One-Day ($\mu\text{g}/\text{m}^3$) | |
|------------------|-----------------|-----------------|--------------------------------------|--------|
| | | | Room-A | Room-C |
| H ₂ S | ≤ 3 | ≈ 0 | 13 | < 12 |
| SO ₂ | ≤ 10 | ≈ 15 | < 10 | < 10 |
| NO ₂ | ≤ 50 | 100-250 | 49 | < 10 |

*Upper bounds are based on $\text{RH} \leq 50\%$.

"<": actual value is below measurement resolution.

can see that the most stringent RH requirement of 85% was violated for limited time periods, while the other two RH requirements of 90% and 100% were never violated. As a comparison, we also investigated the cold air RH in Room-C. Following the common practice, Operator-B sets 20°C and 50% as the temperature and RH setpoints for the hot return air that is inhaled by the CRAC unit. The temperature and RH within the cold air containment is about 17°C and 70% that is represented by the solid horizontal line in Fig. 12. From the figure, we can see that, in fact, the RH of the cold air of Room-C is close to and higher than the average RHs of Room-A's outside and cold air, respectively. Since there is no fault in Room-C, we think high RH alone is not the reason of the faults.

Corrosive gases and particulate contaminations: We investigated the measurements of the corrosive gases and particulate concentration. Two columns of Required and Long-Term of Table 6 show a server vendor's requirements and measurements by gaseous sensors deployed in the testbed, respectively. We can see that the SO₂ concentration is slightly higher than the requirement and the NO₂ concentration is up to 5x higher than the requirement. Since the gas sensors we deployed on our testbed as shown in Fig. 2(i) are designed for real-time long-term monitoring but with less accuracy, we contracted a third-party company with gaseous contaminants monitoring expertise to perform one-day measurements in Room-A and Room-C simultaneously. The company's measurement apparatuses in the two rooms can be found in Fig. 6 in Appendix D. The column of One-Day of Table 6 shows the measurement results. We can see that the NO₂ concentration in Room-A is at least 4.9x higher than that in Room-C. As Room-A and Room-B are about 100 meters from a major highway in our area, we also suspect that the car exhaust gas is a major source of the NO₂. Fig. 13 shows the concentration levels of the fine particles required by ASHRAE and measured by our testbed's PM2.5 sensor during July to September 2019. We can see that the concentration of the fine particles in our testbed is mostly higher than the ASHRAE's requirement level [32]. Singapore is sometimes affected by smoke haze caused by forest fires in the near-by region [33]. As shown in Fig. 13, during the haze period of September 2019, the measured particle concentration in our testbed is much higher than the requirement. On the other hand, Room-C has clean air because DC operators filtrate the air entering the DC building to remove the corrosive gases and particles.

Summary and discussion. As mentioned in Section 2, from the existing research [25], [26], corrosion on metal materials is a joint effect of corrosive gases and RH, because the corrosive gases will absorb moisture in the air to form acids.

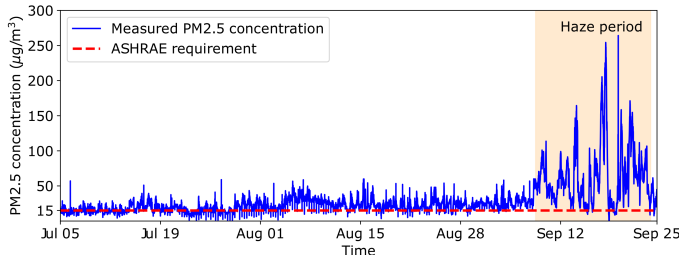


Fig. 13: Concentration of PM2.5 from July to September of 2019 in Room-A.

Particulate contaminants can also attack the metal materials in a similar way or cause short circuit if the ambient RH exceeds the deliquescent RH of the contaminants. The deliquescent RH for many contaminants is about 65% [27]. Note that dust can be seen on the faulty motherboards under microscope during the server vendors' lab-based fault analysis. Therefore, the server faults in Room-A and Room-B can be attributed to (1) the co-presence of NO_2 , dust, and high RH, (2) the lack of anti-corrosion coating for the PCBs in the faulty servers. Note that all the servers tested in our research are designed for enclosed data centers with air filtrated to exclude the air-borne contaminants. The environment in our testbed violated the requirement of the servers, resulting in the server faults.

Room-A and Room-B are about three kilometers from the coastline. ASHRAE's whitepaper [27] mentions that sea salt carried by winds can also damage electronic devices in coastal areas. As there are no mature off-the-shelf sensors to monitor salt concentration in the air, our current research falls short of telling whether sea salt contributed to the server faults. But this issue is of great interest for future research.

6 LEARNED LESSONS AND RECOMMENDATIONS

6.1 Learned Lessons

As the first systematic trial of real air free-cooling for DCs in the tropics, our research has generated various valuable experiences and information for DC-related entities. Some of them are in the form of learned lessons that the future research and industrial practice should consider. The lessons are summarized as follows.

Temperatures up to 37°C do not impede the air free-cooling. Our experiment results based on the testbed show that the servers can operate without computing performance degradation under the cold aisle temperature up to 37°C. The investigation shows that the server faults on our testbed were not caused by temperature. Moreover, many latest servers (e.g., all Dell's gen14 servers and all HPE's DLx gen9 servers) are compliant with the ASHRAE A3 requirement to be able to tolerate 40°C. Thus, the tropics' air temperatures in our area with a record maximum of 37°C will not impede the air free-cooling.

Server hardening vs. airborne contaminants removal. We believe that by deploying hardened IT equipment with anti-corrosion coating on the PCBs exposed to air, hardware faults caused by corrosion and conductive dust can be largely avoided. Alternatively, better airborne contaminants filtration can be employed. The following two categories of

filtration approaches can be considered:

(1) Passive filtration: This project uses Class MERV-6 to remove PM10 and larger particles. Filters in higher classes can be used instead to remove finer particles. For corrosive gases, the hot air generated by the servers can be recirculated and mixed with the outside cold air to form warm air with lower RH to be supplied to the servers. The lower RH will reduce the corrosive gases' attack capabilities. This approach requires no extra energy and exploits the higher temperature tolerance of the latest servers. The details of this approach are described in [29]. The speed control logic of server built-in fans may need adjustment to avoid fast wear and tear due to unnecessarily high rotation speeds in high temperatures. Note that the server fan speed control logic update can be implemented using a shell script and deployed easily.

(2) Active filtration: Electrostatic air cleaners can be employed to strengthen the particle removal. Traditional chemical approaches can be applied to remove corrosive gases. However, these approaches will use energy.

This project narrowed the feasibility problem of air free-cooling in the tropics down to the effectiveness of airborne contaminants removal and its associated Capex and Opex. The choice of server hardening and better filtration is a design problem that will depend on specific configurations and constraints of the DC. For example, server hardening may not be feasible for colocation DCs. We note that carefully choosing the location for cleaner ambient air may significantly ease the design of an air free-cooled DC.

Implication on existing DCs. Our results also suggest that the existing DCs operated in enclosed buildings can consider increasing their temperature setpoints for better energy efficiency if sufficient air flows are provided to the servers to take away generated heat and avoid hot spots. These DCs will not have the airborne contamination problem, owing to the enclosed design and the deployed air filtration systems.

6.2 Recommendations

From the above experiment results, we perform an analysis to make a recommendation on the temperature control for air free-cooled tropical DCs. The DC operators may have different mentalities in accepting high temperatures and their IT devices may have different temperature tolerance levels. Thus, we introduce four temperature control levels, each of which has a specific supply air temperature threshold. The four thresholds are 28°C, 31°C, 34°C, and 37°C. For an air free-cooled tropical DC operating at a certain level, when the outside temperature exceeds the level's recommended temperature threshold, the air free-cooled DC activates the standby cooling coil to process the outside air and maintain the temperature of the air supplied to the servers at the threshold. Otherwise, the outside air is directly blown into the server rooms without additional conditioning. The four temperature thresholds evenly divide the temperature range of [25°C, 37°C] with a step size of 3°C. Such discrete levels facilitate the system implementations and the communications among DC operators and technicians. In Table 7, the second column gives the RH ranges of the supply air under the four levels, which

TABLE 7: Recommendation levels for air free-cooled tropical DCs.

| Level | Supply air temperature threshold | RH range | ASHRAE reliability X-factor [†] | Relative energy saving [‡] |
|---------|----------------------------------|------------------|--|-------------------------------------|
| Level 1 | 28°C | 42.55% to 96.92% | 1.36 | 31.33% |
| Level 2 | 31°C | 35.79% to 96.92% | 1.45 | 56.77% |
| Level 3 | 34°C | 32.99% to 96.92% | 1.52 | 53.36% |
| Level 4 | 37°C | 29.55% to 96.92% | 1.6 | 53.48% |

[†]The X-factor of each level is interpolated using the ASHRAE’s X-factor data for the supply air temperature threshold.

[‡]The relative energy saving achievable with the energy usage at 25°C as the baseline.

are obtained by a set of simulations that are driven by the 15-month outside air temperature and RH traces collected from our testbed. A simulation is performed as follows. When the outside temperature is lower than the temperature threshold, the supply air RH is the outside air RH. When the cooling coil is activated, the supply air RH ϕ_s is determined based on the supply air temperature threshold t_s , outside air temperature t_o and RH ϕ_o using the following psychrometric equation [34]: $\phi_s = \phi_o \frac{f(t_o+273.15)}{f(t_s+273.15)}$, where $f(x) = \exp(c_0 - \frac{c_1}{x} - c_2x + c_3x^2 - c_4x^3 + c_5 \ln x)$. Note that c_i ($i = 1, \dots, 5$) are constant coefficients that characterize the psychrometrics of the air processes in the cooling coil.

Due to the limited number of tested servers, the experimental results collected from the testbed do not allow us to derive a reliability metric which characterizes the impact of the temperature on the IT hardware reliability. Thus, for the IT hardware reliability at each recommended level, we adopt the relative failure rates of IT equipment under certain temperatures, called X-factors which are provided by ASHRAE to guide the choice of DC temperature setpoint [5]. The column of ASHARE reliability X-factor is the X-factors corresponding to the level’s supply air temperature threshold. The X-factors can be used to interpolate the impact of the temperature on the reliability as follows. For instance, at Level 4, the X-factor is 1.6, meaning that the failure rate at 37°C is 1.6 times of the failure rate at the reference temperature of 20°C. A cloud service provider’s statistics [35] reported 1.25% as the baseline annualized failure rate (AFR) of HDDs at 20°C. As a result, the maximum AFR at Level 4 with the threshold of 37°C is $1.25\% \times 1.6 = 2\%$, i.e., two out of 100 HDDs fail over one year. As discussed in Section 4.3.1, the supply air temperature from 25°C to 37°C has similar impact on the server computing performance. The servers can operate without computing performance degradation under the temperature up to 37°C. Thus, we do not include the server computing performance metric for each recommendation level in Table 7. Furthermore, the last column of Table 7 shows the relative energy savings achieved at the temperature thresholds with the energy usage at 25°C as the baseline. From the table, we can see that the energy saving achieves a knee point when the temperature control threshold is 31°C. With higher temperature threshold, the energy saving has a slight reduction. This is because the servers’ built-in fans will rotate faster, resulting in higher energy usage.

We cross check the simulated temperature and RH traces against ASHRAE’s four classes regarding IT equipment’s temperature/RH tolerance. Fig. 14 shows the relationship

between our recommended temperature control levels and the ASHRAE’s four classes of IT equipment’s temperature and RH tolerance. Specifically, for each level of our recommendation, we check whether the temperature requirement of each ASHRAE class is satisfied and also the percentage of time in Singapore’s context when the ASHRAE class’ RH requirement is satisfied. From Fig. 14, we can see that Level 2, 3, and 4 are compatible with the ASHRAE class A3. Moreover, by jointly analyzing the results in Fig. 14 and Table 7, we can achieve a rule-of-thumb recommendation of adopting ASHRAE Class A3 IT equipment and running the air free-cooled tropical DC at Level 3 with the temperature threshold of 31°C. With this configuration, we can fully meet ASHRAE’s A3 temperature requirement, meet A3 RH requirement for 96.5% of time, and achieve the highest energy saving of 56.77%. Note that many latest servers (e.g., all Dell’s gen14 servers and all HPE’s DLx gen9 servers) are compliant with the class A3 requirement. It is important to note that this rule-of-thumb recommendation does not override the need of clean air and/or anti-corrosion measures, since the ASHRAE’s A3 requirement assumes clean air.

7 CONCLUSION

In this paper, we describe the design, construction, and configuration of an air free-cooled DC testbed in the tropical condition. We also present the key results of the experiments conducted on the testbed, including the energy efficiency of the air free-cooling facility, servers’ computing performance, server faults during the experiments, and the investigations on the reasons of the faults. The experiences, learned lessons, and the recommendations discussed in this paper will be useful to future efforts of building and operating air free-cooled DCs in the tropics and beyond, aiming at increasing the DC energy efficiency while not compromising the server performance and reliability.

ACKNOWLEDGMENTS

This project is a collaboration between Info-communications Media Development Authority and Nanyang Technological University of Singapore. This project is supported by the National Research Foundation, Prime Minister’s Office, Singapore under its Green Data Centre Programme. The authors acknowledge Yew-Wah Wong and Dr. Yonggang Wen for their valuable inputs. The authors acknowledge the contributions from the following partners (names not listed in order): Dell EMC, Epsilon, ERS Industries, Fujitsu,

| Level | ASHRAE Classes | | | | | | | |
|---------------------|----------------|----------------------------------|--------------|----------------------------------|-------------|---------------------------------|-------------|---------------------------------|
| | A1 | | A2 | | A3 | | A4 | |
| | [15°C, 32°C] | Compliance with RH of [20%, 80%] | [10°C, 35°C] | Compliance with RH of [20%, 80%] | [5°C, 40°C] | Compliance with RH of [8%, 85%] | [5°C, 45°C] | Compliance with RH of [8%, 90%] |
| Level 1 (≤ 28°C) | ✓ | 38.3% | ✓ | 38.3% | ✓ | 78.4% | ✓ | 97.2% |
| Level 2 (≤ 31°C) | ✓ | 84.3% | ✓ | 84.3% | ✓ | 96.5% | ✓ | 99.4% |
| Level 3 (≤ 34°C) | ✗ | 84.3% | ✓ | 84.3% | ✓ | 96.5% | ✓ | 99.4% |
| Level 4 (≤ 37°C) | ✗ | 84.3% | ✗ | 84.3% | ✓ | 96.5% | ✓ | 99.4% |

Fig. 14: Relationship between different levels of temperature control and ASHRAE's classes.

Future Facilities, Hewlett Packard Enterprise, Huawei, IX Technologies, Keppel Data Centres, Singtel, Intel, Micron, National University of Singapore, The Green Grid, and Uptime Institute. Rui Tan's work is also supported by an MOE AcRF Tier 1 grant (2019-T1-001-044).

REFERENCES

- [1] D. Van Le, Y. Liu, R. Wang, R. Tan, and L. H. Ngoh, "Experiences and learned lessons from an air free-cooled tropical data center testbed," in *ACM BuildSys*, 2020, pp. 160–169.
- [2] Singapore's Info-communications Media Development Authority, "Green Data Centre Technology Roadmap," <https://bit.ly/2Sj2f6x>, 2014.
- [3] W. Wong, "Singapore's Colocation Market to Nearly Double by 2023," <https://bit.ly/3hMYPmX>, 2019.
- [4] Hainan Zhang, Shuangquan Shao, Hongbo Xu, Huiming Zou, Changqing Tian, "Free cooling of data centers: A review," *Renew. Sust. Energ. Rev.*, vol. 35, pp. 171–182, 2014.
- [5] ASHRAE TC 9.9, "Thermal guidelines for data processing environments," *White Paper*, 2011.
- [6] J. Park, "Designing a very efficient data center," <https://bit.ly/2xBE7Oj>, 2011.
- [7] Y. Sverdlik, "Free cooling inspires google data center murals in dublin," <https://bit.ly/2VvGNgy>, 2017.
- [8] T. Harvey, M. Patterson, and J. Bean, "Updated air-size free cooling maps: The impact of ASHRAE 2001 allowable ranges," *White Paper*, 2012.
- [9] A. Habibi Khalaj, T. Scherer, and S. K. Halgamuge, "Energy, environmental and economical saving potential of data centers with various economizers across australia," *Applied Energy*, vol. 183, 2016.
- [10] S.-W. Ham, J.-S. Park, and J.-W. Jeong, "Optimum supply air temperature ranges of various air-side economizers in a modular data center," *Applied Thermal Engineering*, pp. 163 – 179, 2015.
- [11] Y. Udagawa, S. Waragai, M. Yanagi, and W. Fukumitsu, "Study on free cooling systems for data centers in Japan," in *INTELEC*, 2010.
- [12] V. Depoorter, E. Oró, and J. Salom, "The location as an energy efficiency and renewable energy supply measure for data centres in europe," *Applied Energy*, vol. 140, pp. 338–349, 2015.
- [13] J. Siriwardana, W. Y. Wah, T. K. Chuan, and W. Yonggang, "Optimisation of outdoor air cooling system for modular data center," in *The SB 13 Singapore - Realising Sustainability in the Tropics*, 2013.
- [14] H. Endo, H. Kodama, H. Fukuda, T. Sugimoto, T. Horie, and M. Kondo, "Effect of climatic conditions on energy consumption in direct fresh-air container data centers," *Sustainable Computing: Informatics and Systems*, vol. 6, pp. 17–25, 2015.
- [15] K. Heslin, "2014 data center industry survey," <https://bit.ly/2K1UDz4>, 2015.
- [16] "Google cluster workload traces," <https://bit.ly/3vh9YR2>, 2020.
- [17] "Alibaba cluster trace program," <https://bit.ly/3wvFQBN>, 2019.
- [18] A. Habibi Khalaj and S. K. Halgamuge, "A review on efficient thermal management of air- and liquid-cooled data centers: From chip to the cooling system," *Applied Energy*, vol. 205, pp. 1165 – 1188, 2017.
- [19] J. Siriwardana, S. Jayasekara, and S. K. Halgamuge, "Potential of air-side economizers for data center cooling: A case study for key australian cities," *Applied Energy*, vol. 104, pp. 207–219, 2013.
- [20] N. El-Sayed, I. A. Stefanovici, G. Amvrosiadis, A. A. Hwang, and B. Schroeder, "Temperature management in data centers: why some (might) like it hot," *ACM SIGMETRICS Performance Evaluation Review*, vol. 40, no. 1, pp. 163–174, 2012.
- [21] S. Sankar, M. Shaw, K. Vaid, and S. Gurumurthi, "Datacenter scale evaluation of the impact of temperature on hard disk drive failures," *ACM Transactions on Storage*, vol. 9, no. 2, p. 6, 2013.
- [22] I. Manousakis, S. Sankar, G. McKnight, T. D. Nguyen, and R. Bianchini, "Environmental conditions and disk reliability in free-cooled datacenters," in *USENIX FAST*, 2016, pp. 53–65.
- [23] J. Srinivasan, S. V. Adve, P. Bose, and J. A. Rivers, "The case for lifetime reliability-aware microprocessors," in *31st Annual International Symposium on Computer Architecture*, 2004, pp. 276–287.
- [24] E. Pinheiro, W.-D. Weber, and L. A. Barroso, "Failure trends in a large disk drive population," in *USENIX FAST*, 2007, pp. 2–2.
- [25] P. Singh, L. Klein, D. Agonafer, J. Shah, and K. Pujara, "Effect of relative humidity, temperature and gaseous and particulate contaminations on information technology equipment reliability," in *InterPACK*, 2015, pp. 1–9.
- [26] J.-E. Svensson and L.-G. Johansson, "A laboratory study of the effect of ozone, nitrogen dioxide, and sulfur dioxide on the atmospheric corrosion of zinc," *Journal of the Electrochemical Society*, vol. 140, no. 8, pp. 2210–2216, 1993.
- [27] ASHRAE, "Gaseous and particulate contamination guidelines for data centers," *White Paper*, 2011.
- [28] L. Li, W. Zheng, X. Wang, and X. Wang, "Coordinating liquid and free air cooling with workload allocation for data center power minimization," in *ICAC*, 2014, pp. 249–259.
- [29] D. V. Le, R. Wang, Y. Liu, R. Tan, Y.-W. Wong, and Y. Wen, "Deep reinforcement learning for tropical air free-cooled data center control," *ACM Transactions on Sensor Networks (TOSN)*, vol. 17, no. 3, pp. 1–28, 2021.
- [30] V. Avelar, D. Azevedo, A. French, and E. N. Power, "PUE: a comprehensive examination of the metric," *White paper*, 2012.
- [31] D. V. Le, Y. Liu, R. Wang, and R. Tan, "Tropical data centre proof-of-concept," <https://bit.ly/3sdwXf5>, Technical Report, 2020.
- [32] American Society of Heating, Refrigerating and Air-Conditioning Engineers, Inc., *Design Consideration for Datacom Equipment Centers*, 2009, ch. 8.
- [33] S. N. E. Agency, "Magaging haze," <https://bit.ly/3oCSCM2>, May 25, 2020.
- [34] American Society of Heating, Refrigerating and Air-Conditioning Engineers, Inc., *2013 ASHRAE Handbook - Fundamentals (SI Edition)*, 2017, ch. 1.
- [35] "Backblaze hard drive stats for 2018," <https://bit.ly/2T8BiOa>.



Duc Van Le is a Research Fellow at School of Computer and Engineering, Nanyang Technological University, Singapore. Previously, he was a Research Fellow (2016-2018) at Department of Computer Science, National University of Singapore. He received the Ph.D. (2016) degree in computer engineering from University of Ulsan, South Korea, and the B.Eng. (2011) degree in electronics and telecommunications engineering from the Le Quy Don Technical University, Vietnam. His research interests include sensor networks, cyber-physical systems and mobile/edge sensing and computing. He is a member of the IEEE.

works, cyber-physical systems and mobile/edge sensing and computing. He is a member of the IEEE.



Yingbo Liu is an Assistant Researcher at Yunnan University of Finance and Economics. He is the Director of the Cloud Computing Center of Big Data Research Institute of Yunnan Economy and Society. He was a postdoctoral researcher at Yunnan Academy of Scientific & Technical Information (2015-2018) and a Research Fellow at SCSE of NTU, Singapore (2018-2019). He obtained his Ph.D. degree from the University of Chinese Academy of Sciences (2015), M.S. degree (2011) in Computer Science and Application and B.S. degree (2008) in Automation from Kunming University of Science and Technology. His research interests include big data, cloud computing, and distributed systems.

obtained his Ph.D. degree from the University of Chinese Academy of Sciences (2015), M.S. degree (2011) in Computer Science and Application and B.S. degree (2008) in Automation from Kunming University of Science and Technology. His research interests include big data, cloud computing, and distributed systems.



Rongrong Wang is currently a Ph.D. student in School of Computer Science and Engineering (SCSE) at Nanyang Technological University (NTU), Singapore. She received her B.Eng (2017) in Control Science and Engineering from Northwestern Polytechnical University in China, and M.S. (2018) in electrical and electronic engineering from NTU. She is now a Research Associate at SCSE, NTU. Her research interests include advanced sensing and smart CPS environment.



Rui Tan is an Associate Professor at School of Computer Science and Engineering, Nanyang Technological University, Singapore. Previously, he was a Research Scientist (2012-2015) and a Senior Research Scientist (2015) at Advanced Digital Sciences Center, a Singapore-based research center of University of Illinois at Urbana-Champaign, and a postdoctoral Research Associate (2010-2012) at Michigan State University. He received the Ph.D. (2010) degree in computer science from City University of Hong

Kong, the B.S. (2004) and M.S. (2007) degrees from Shanghai Jiao Tong University. His research interests include cyber-physical systems, sensor networks, and pervasive computing systems. He is the recipient of IPSN'21 Best Artifact Award Runner-Up, IPSN'17 and CPSR-SG'17 Best Paper Awards, IPSN'14 Best Paper Award Runner-Up, PerCom'13 Mark Weiser Best Paper Award Finalist, and CityU Outstanding Academic Performance Award. He is currently serving as an Associate Editor of the ACM Transactions on Sensor Networks. He also serves frequently on the technical program committees (TPCs) of various international conferences related to his research areas, such as SenSys, IPSN, and IoTDI. He received the Distinguished TPC Member recognition twice from INFOCOM in 2017 and 2020. He is a Senior Member of IEEE.



Lek Heng Ngoh, Ph.D. is an executive manager of Infrastructure Development division at Infocomm Media Development Authority (IMDA) of Singapore. His current job scope involves initiating and managing data centre and cloud computing related projects. Lek Heng was the project manager of Tropical Data Centre Proof-of-Concept trials conducted from Dec 2017 to Dec 2019.

Supplementary File

Duc Van Le, Yingbo Liu, Rongrong Wang, Rui Tan, and Lek Heng Ngho

This document includes the supplemental materials for the paper titled “Air Free-Cooled Tropical Data Center: Design, Evaluation, and Learned Lessons”.

APPENDIX A ENERGY USAGE AND ENVIRONMENTAL CONDITION DATASET

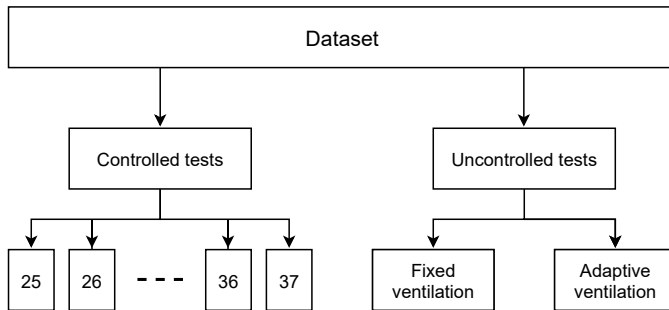


Fig. 1: Data folder organization.

We provide a sensor measurement dataset¹ collected from our air free-cooled DC testbed to the research communities. Specifically, the dataset can be divided into two categories: energy and environmental data which are measured by instrumented hardware and software sensors during the controlled and uncontrolled tests. Fig. 1 shows the folder organization of the dataset. Specifically, the data files are grouped into two main folders: controlled and uncontrolled tests. The controlled tests folder includes 13 subfolders, each of which includes the sensor measurements under a specific supply temperature setpoint from 25°C to 37°C. The uncontrolled tests folder include 2 sub-folders: adaptive ventilation and fixed ventilation. Furthermore, each subfolder includes multiple sensor measurement files which are recorded as time-series data. Each data point is indexed by a timestamp corresponding to when the sensor measurement is sampled. Table 1 describes the content of each sensor measurement files in each subfolder.

APPENDIX B PSYCHROMETRIC EQUATIONS

Let’s define the following notation: t is temperature; ϕ is RH; f is volume flow rate; h is enthalpy; w is moisture

content and \dot{m} is mass flow rate. For these psychrometric variables, we use the subscripts \cdot_o , \cdot_c , \cdot_s , \cdot_h and \cdot_{wv} to refer to the outside air, the saturated air leaving the cooling coil, the supply air in the cold aisle, the hot air in the hot aisle, and the water vapor removed from the outside air by the cooling coil, respectively. The supply air condition can be determined using mass and energy conservation equations which characterize the psychrometrics of air heating, cooling and mixing processes in the cooling-then-mixing approach as follows.

(1) Heating: Since the hot air carries the heat generated by the servers, the enthalpy h_h of the return air is higher than that of the supply air h_s . Moreover, the servers do not add extra moisture to the air. Thus, the moisture contents at the cold and hot aisles are identical. Moreover, the servers do not change the air mass flow rate. Let p_{IT} and β denote the servers’ total power and heat rate transfer coefficient. The psychrometrics of the heating process in the server room is

$$\dot{m}_h h_h = \dot{m}_s h_s + \beta p_{IT}, \quad \dot{m}_h = \dot{m}_s, \quad w_h = w_s. \quad (1)$$

(2) Cooling: The cooling coil first reduces the temperature of the incoming outside air to the dewpoint temperature of t_d without condensation. Then, moisture condensation will occur when the cooling coil continues to cool the air to temperature below the t_d until the final saturated temperature t_c . Denoting by $q_c \geq 0$ the total heat rate removed by the cooling coil, the mass and energy conservation equations of the psychrometric processes in the cooling coil are

$$\dot{m}_o h_o = \dot{m}_{wv} h_{wv} + \dot{m}_c h_c + q_c, \quad \dot{m}_o w_o = \dot{m}_{wv} + \dot{m}_c w_c. \quad (2)$$

(3) Mixing: The cooled and dried air leaving the cooling coil is mixed with the hot air in the mixing chamber to form the air supplied to the servers. Let $\alpha \in [0, 1]$ denote the portion of the recirculated hot air in the supply air. Then, $1 - \beta$ is the portion of the outside air in the supply air. Characterized by the conservation of the mass and energy in the mixing process, the condition of the supply air is

$$\begin{cases} h_s &= (1 - \alpha)h_c + \alpha h_h, \\ w_s &= (1 - \alpha)w_c + \alpha w_h, \\ \dot{m}_s &= (1 - \alpha)\dot{m}_c + \alpha \dot{m}_h. \end{cases} \quad (3)$$

Note that in above Eqs. (1)-(3), the air condition in each air processing step is characterized by the enthalpy h , moisture content w and mass flow rate \dot{m} . The temperature t °C, RH ϕ (%) and volume flow rate f (m³/s) can be calculated using these variables h (kJ/kg), w (kg/kg) and \dot{m} (kg/s)

1. Publicly available at <https://bit.ly/31sWPKS>

TABLE 1: Description of dataset files.

| File | Description |
|--|--|
| Energy_PUE.csv | Instantaneous PUE |
| Energy_Fan.csv | Powers of supply and exhaust fans |
| Energy_Heater.csv | Power of heater |
| Energy_Rack.csv | Powers of four IT racks |
| Energy_AirCon.csv | Powers of cooling coils and supporting facilities |
| Airflow_Control.csv | Supply air flow rate setpoint and measurement |
| Chemical.csv | Concentrations (ppb) of NO ₂ , H ₂ S and SO ₂ |
| PM2.5.csv | Concentrations ($\mu\text{g}/\text{m}^3$) of PM2.5 |
| DP_Rack_1.csv and DP_Rack_2.csv | Differential pressure across IT racks |
| Outside_Temp_RH.csv | Outside air temperature, RH and dewpoint |
| RH_Cold_Rack_1.csv, RH_Cold_Rack_2.csv | Supply air RH in front of four IT racks |
| RH_Hot_Rack_1.csv, RH_Hot_Rack_2.csv | Hot air RH in back of four IT racks |
| Temp_Cold_Rack_1.csv, Temp_Cold_Rack_2.csv | Supply air temperature in front of four IT racks |
| Temp_Hot_Rack_1.csv, Temp_Hot_Rack_2.csv | Hot air temperature in back of four IT racks |
| Temp_Control.csv | Supply air temperature setpoint and measurement |
| Temp_Room.csv | Temperature at mixing, cold, hold and buffer spaces |
| RH_Room.csv | RH at mixing, cold, hold and buffer spaces |

as follows [1].

$$t = \frac{h - 2501w}{1.006 + 1.86w}, \quad \phi = \frac{p_w}{p_{ws}} \times 100\%, \quad f = \frac{\dot{m}}{\rho}, \quad (4)$$

where ρ (kg/m^3) is the air density, p_w (Pa) is the water vapor pressure and p_{ws} (Pa) is the saturation pressures. The relationship of p_w and p_{ws} with the w and t can be expressed as

$$\begin{cases} w &= 0.621945 \frac{p_w}{\rho - p_w}, \\ \ln p_{ws} &= c_1 + \frac{c_2}{t} + c_3 t + c_4 t^2 + c_5 t^3 + c_6 \ln t, \end{cases} \quad (5)$$

where $c_1 = -5.8002206 \times 10^3$, $c_2 = 1.3914993$, $c_3 = -4.8640239 \times 10^{-2}$, $c_4 = 4.1764768 \times 10^{-5}$, $c_5 = -1.4452093 \times 10^{-8}$, $c_6 = 6.5459673$.

More details about above Psychrometric equations and coefficients can be found in [1].

APPENDIX C SERVER COMPUTING PERFORMANCE

C.1 CPU Test Results

We measured giga floating point operations per second (GFLOPS) to characterize the CPU performance. We also monitored the CPU core frequency to pinpoint performance degradation caused by frequency throttling. The tests show that, for all CPUs in Room-A and Room-B, the temperature setpoint has little/no impact on GFLOPS and core frequency when (1) the temperature setpoint is from 25°C and 37°C, (2) the CPU utilization is from 10% to 90%, and (3) the air volume flow rate is 2500 m³/h and above. We also investigated the thermal safety of the tested CPUs. The vendor of the tested CPUs specifies \bar{T}_{case} for each CPU model, which is the upper limit of the CPU *case temperature* for thermal safety. However, each CPU only has a built-in digital thermal sensor to measure T_{core} , which is the *core temperature* on the die. During the tests, the measured T_{core} was always below \bar{T}_{case} . As the case temperature is always lower than the core temperature, the case temperature, although inaccessible, must be lower than \bar{T}_{case} . Thus, all the tested CPUs were

thermally safe during the CPU tests in Room-A and Room-B. This also explains the absence of core frequency throttling in the tests. An expert representative from the CPU vendor agreed the above results.

C.2 HDD Test Results

We measured the input/output operations per second (IOPS) and response time during random read and write accesses to characterize the HDD performance. The tests show that, for all HDDs in Room-A and Room-B, the temperature setpoint has little/no impact on IOPS and response time when (1) the temperature setpoint is from 25°C to 37°C, (2) the HDD random read/write speed is from 10 MB/s to 100 MB/s, and (3) the air volume flow rate is from 2500 m³/h to 12500 m³/h. The results also show that the HDD random read/write speed has little impact on the server energy usage.

C.3 Memory Test Results

We measured the speed of copying a large amount of data from a user space memory area to another area using various block sizes to characterize the memory performance. We use cyclic redundancy check (CRC) to verify the integrity of the data copying. The tests show that, for all memories in Room-A and Room-B, the temperature setpoint has little/no impact on memory speed when (1) the temperature setpoint is from 25°C to 37°C, (2) the block size setting is from 8 kB to 256 kB, and (3) the air volume flow rate is from 2500 m³/h to 12500 m³/h. No CRC verification errors occurred during the tests. The results also show that the memory speed has little impact on the server energy usage.

C.4 Node Test Results

We tested the CPU, HDD, and memory simultaneously under a total of six server status levels. At the first level where the server has light workload and the sixth level where the server is stressed, the CPU utilization, HDD

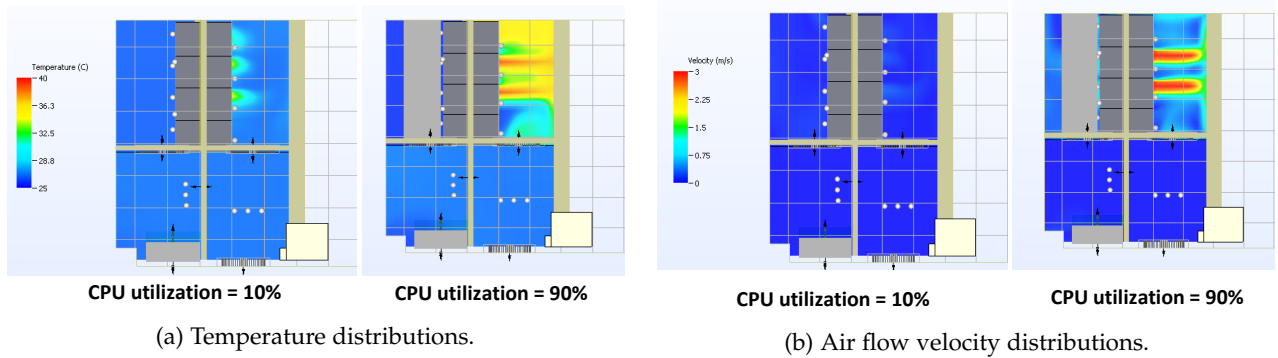


Fig. 2: Temperature and air flow velocity distributions in Room-A that are generated by CFD simulations. The supply air temperature setpoint is set to 26°C.

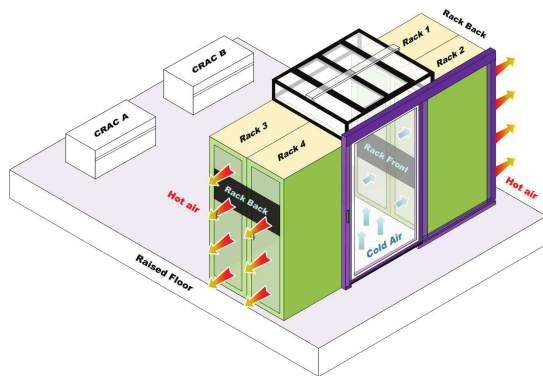


Fig. 3: Design of Room-C and cold air containment.

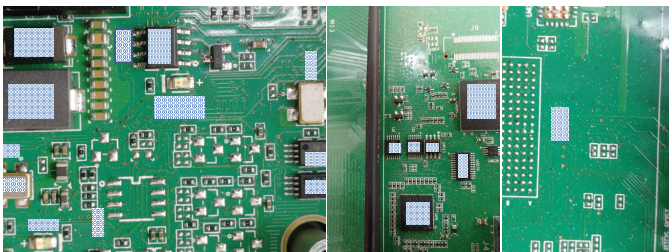


Fig. 4: Dusts rest on the PCBs of the motherboard.



Fig. 5: Microscopic images of corrosion on server PCBs and components.



Fig. 6: Simultaneous precise one-day measurement of corrosive gases concentrations in Room-A and Room-C.

read/write speed, and memory block size in data copying are {10%, 10 MB/s, 8 kB} and {90%, 100 MB/s, 256 kB}, respectively. The test results show that the performance metrics of CPU, HDD, and memory are similar to those tested separately, except that the memory speed is affected by CPU utilization setpoint. This is because CPU cycles are needed to copy data for testing the memory. In contrast, the HDD performance is not affected by CPU utilization setpoint, because HDD is a low-speed device compared with CPU and memory. All the CPUs were also thermally safe, although CPU, HDD, and memory generate heat simultaneously.

**APPENDIX D
FIGURES**

Fig. 2 shows the results of the CFD models simulations regarding the temperature and air flow velocity distribu-

tions under the supply air temperature setpoint of 26°C and different server CPU utilization levels in Room-A. Fig. 3 illustrates the layout of Room-C with an air containment and the air flows. Fig. 4 shows several pinpointed corrosion problems that caused the mainboard failures. Fig. 5 shows the dusts resting on the PCBs of the motherboards of the faulty servers. We contracted a third-party company with gaseous contaminants monitoring expertise to perform one-day measurements in Room-A and Room-C simultaneously. Fig. 6 shows the company’s measurement apparatuses in the two rooms.

REFERENCES

[1] American Society of Heating, Refrigerating and Air-Conditioning Engineers, Inc., *2013 ASHRAE Handbook - Fundamentals (SI Edition)*, 2017, ch. 1.